Liraglutide Treatment Reverses Unconventional Cellular Defects in Induced Pluripotent Stem Cell–Derived β-Cells Harboring a Partially Functional *WFS1* Variant

Silvia Torchio,[1,2] Gabriel Siracusano,[1,2] Federica Cuozzo,[1] Valentina Zamarian,[1] Silvia Pellegrini,[1] Fabio Manenti,[1] Riccardo Bonfanti,[3] Giulio Frontino,[3] Valeria Sordi,[1] Raniero Chimienti,[1,2] and Lorenzo Piemonti[1,2]

Diabetes 2025;74:1273–1288 | https://doi.org/10.2337/db24-0720

Wolfram syndrome 1 (WS1) is a rare genetic disorder caused by *WFS1* variants that disrupt wolframin, an endoplasmic reticulum-associated protein essential for cellular stress responses, Ca^{2+} homeostasis, and autophagy. Here, we investigated how the c.316-1G>A and c.757A>T *WFS1* mutations, which yield partially functional wolframin, affect the molecular functions of β-cells and explored the therapeutic potential of the glucagon-like peptide 1 receptor (GLP-1R) agonist liraglutide. Pancreatic β-cells obtained from patient-derived induced pluripotent stem cells (iPSCs) carrying this *WFS1* variant exhibited reduced insulin processing and impaired secretory granule maturation, as evidenced by proinsulin accumulation and decreased prohormone convertase PC1/3. Moreover, they exhibited dysregulated Ca^{2+} fluxes due to altered transcription of Ca^{2+}-related genes, including *CACNA1D*, and significantly reduced *SNAP25* levels, leading to uncoordinated oscillations and poor glucose responsiveness. Affected cells also showed increased autophagic flux and heightened susceptibility to inflammatory cytokine-induced apoptosis. Notably, liraglutide treatment rescued these defects by normalizing Ca^{2+} handling, enhancing insulin processing and secretion, and reducing apoptosis, likely through modulation of the unfolded protein response. These findings underscore the importance of defining mutation-specific dysfunctions in WS1 and support targeting the GLP-1/GLP-1R axis as a therapeutic strategy.

ARTICLE HIGHLIGHTS

- The molecular basis of *WFS1*-related mutations remains poorly investigated, and no definitive therapies exist for Wolfram syndrome 1.
- We dissected the molecular defects associated with c.316-1G>A and c.757A>T *WFS1* mutations in patient-derived induced pluripotent stem cell islets and analyzed whether they are potential therapeutic targets of the glucagon-like peptide 1 receptor agonist liraglutide.
- We found impaired insulin granule maturation, altered Ca^{2+} fluxes, increased autophagic activity, and heightened susceptibility to inflammatory apoptosis in mutated cells.
- Liraglutide restored critical β-cell functions suggesting a route for personalized therapy based on *WFS1* mutations.

Wolfram syndrome 1 (WS1) is a rare autosomal recessive disease characterized by childhood-onset diabetes and optic atrophy, followed by hearing loss, diabetes insipidus, urinary dysfunctions, and ultimately leading to premature death (1). The disease is caused by pathogenic variants in the *WFS1* gene, which encodes wolframin, a transmembrane endoplasmic reticulum (ER) protein involved in ER stress

[1]Unit of β Cell Biology, Diabetes Research Institute, IRCCS San Raffaele Hospital, Milan, Italy
[2]Vita-Salute San Raffaele University, Milan, Italy
[3]Department of Pediatrics, IRCCS San Raffaele Hospital, Milan, Italy

Corresponding authors: Lorenzo Piemonti, piemonti.lorenzo@hsr.it, Raniero Chimienti, chimienti.raniero@hsr.it, and Silvia Torchio, silvia.torchio@curie.fr

Received 22 August 2024 and accepted 7 April 2025

This article contains supplementary material online at https://doi.org/10.2337/figshare.28742351.

S.T. and G.S. are joint first authors.

R.C. and L.P. are joint last authors.

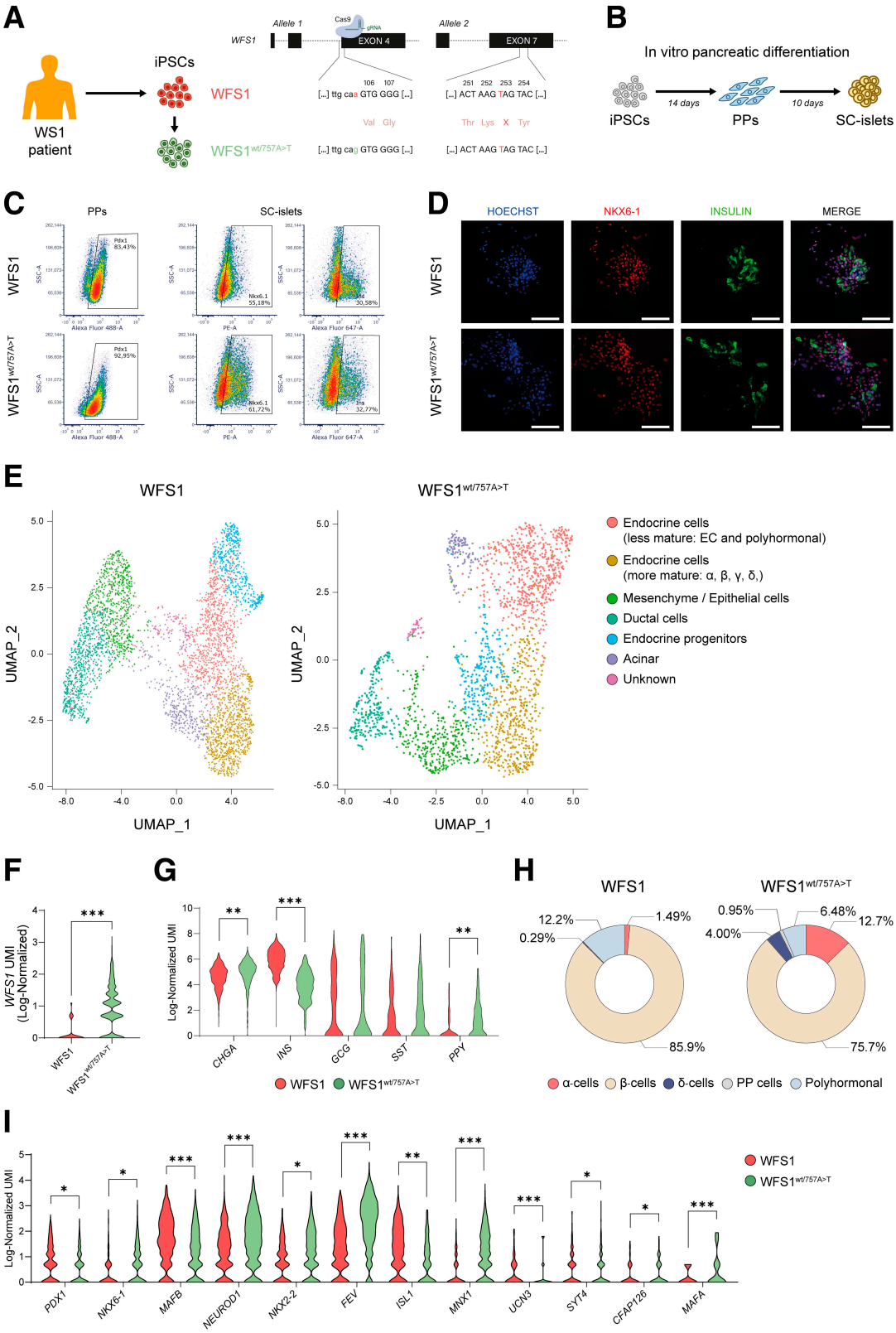

Figure 1—Endocrine phenotype of WFS1 SC islets. *A*: Schematic summary of iPSC generation from patient with WS1 and gene targeting for Cas9 correction of the c.316G>A-carrying allele. *B*: Schematic of differentiation protocol mimicking development of pancreatic progenitors (PPs) and pancreatic β-cells (SC islets). *C*: Representative flow cytometry dot plots showing the percentage of PDX1^{+}, NKX6-1^{+}, and INS^{+} cells in WFS1 and WFS1$^{wt/757A>T}$ at the PP and SC islets stages. PE, phycoerythrin; SSC, side scatter. *D*: Immunostaining of WFS1 and WFS1$^{wt/757A>T}$ SC islets stained for NKX6-1 and insulin. Nuclei were counterstained with Hoechst. Scale bar is 100 μm. *E*: Uniform Manifold Approximation and Projection (UMAP) from unsupervised clustering of transcriptional data from scRNA-seq of WFS1 and WFS1$^{wt/757A>T}$ SC islets. *F*: Violin plots detailing log-normalized unique molecular identifiers (UMIs) of *WFS1* gene in WFS1

regulation (2). In pancreatic β-cells, wolframin also modulates insulin biosynthesis, Ca^{2+} homeostasis, and autophagy, preserving survival and function (3–6). WS1 β-cells display reduced insulin secretion, elevated proinsulin-to-insulin ratio, and are highly susceptible to stress-induced apoptosis (7–9). Despite various preclinical and clinical efforts, no definitive therapy is available (8,10,11). Multiple drug repurposing strategies, focusing on chemical chaperones, ER Ca^{2+} stabilizers, and stress-targeted compounds, have been explored, but clinical evidence of delayed disease progression remains elusive (10).

Growing evidence supports glucagon-like peptide 1 receptor (GLP-1R) agonists as promising alternatives, given their pleiotropic effects on different tissues (12) and multiple processes, including ER stress (13), autophagy (14), Ca^{2+} handling (15), and β-cell–specific processes such as insulin secretion (16). An off-label clinical trial in pediatric WS1 patients showed liraglutide was well tolerated, slowing pancreatic endocrine and neuronal deterioration (17). Similarly, dulaglutide reversed glucose intolerance in wolframin-deficient mice, while exenatide and dulaglutide improved β-cell function in WS1-induced pluripotent stem cells (iPSC)–derived β-cells (18). However, how specific *WFS1* variants alter β-cell function and GLP-1R agonists reverse these defects remains insufficiently explored.

We previously characterized a WS1 patient harboring two compound heterozygous *WFS1* variants (c.316-1G>A and c.757A>T) associated with diabetes, optic atrophy, and a chronic inflammatory state (17,19,20). The c.316-1G>A allele yields multiple transcripts, including some with premature termination codons (PTC) subjected to nonsense-mediated decay and others retaining a functional wolframin C-terminus. Under inflammatory conditions and exogenous stress, PTC-containing transcripts accumulate and drive β-cell death (20). Yet, the specific functional consequences of these *WFS1* variants and whether GLP-1R agonists can mitigate the resulting β-cell defects have not been fully investigated.

In this study, we examined the molecular mechanisms underlying dysfunction in iPSC-derived β-cells from this WS1 patient and explored how the GLP-1R agonist liraglutide might counteract the altered cellular pathways. Our findings strengthen use of liraglutide as a promising therapeutic option for WS1 and feature the potential for personalized or alternative treatments based on specific *WFS1* mutations.

RESEARCH DESIGN AND METHODS

Cell Culture

Two WFS1 and three WFS1$^{wt/757A>T}$ iPSC clones from a female WS1 patient were previously described (20) and tested negative for mycoplasma (MycoAlert, Lonza). Pancreatic β-cell differentiation followed a published protocol (20). At the final stage, iPSC-derived β-cells (SC islets) were detached with 0.5 mmol/L EDTA, transferred to Petri dishes, and kept in suspension culture using CMRL 1066 medium supplemented with 10% FBS, 1% penicillin/streptomycin, 1% L-glutamine, 10 μmol/L Alk5i II, 1 μmol/L T3, 10 mmol/L nicotinamide, 10 μmol/L H1152, and 100 units/mL DNase I. Exogenous stress was induced by 50 or 500 nmol/L thapsigargin (8–16 h) or proinflammatory cytokines (1,000 units/mL interferon-γ, 10 ng/mL tumor necrosis factor-α, and 50 units/mL interleukin-1β, for 48 h). For autophagy assessment, 100 nmol/L bafilomycin A1 was applied for 2 h. For apoptosis studies, 1 μmol/L liraglutide was added concomitantly to thapsigargin or cytokines.

Flow Cytometry

SC islets were dissociated with trypsin, and live cells were identified with LIVE/DEAD Fixable Violet (Thermo Fisher Scientific). Following fixation (Cytofix/Cytoperm, BD Biosciences) and permeabilization (Phosflow Perm Buffer III), cells were stained with intracellular antibodies (Supplementary Table 1). Apoptosis was assessed using propidium iodide and FITC annexin V (BD Biosciences). Data were collected on a FACS Canto (BD Biosciences) and analyzed with FlowJo 10 software.

Immunofluorescence

SC islets were fixed with 4% paraformaldehyde in PBS for 20 min at room temperature, quenched in 15 mmol/L glycine, and permeabilized/blocked in PBS with 0.4% Triton X-100, 2% BSA, and 5% FBS. Primary antibodies (Supplementary Table 1) were applied overnight at 4°C, followed by secondary antibodies (Supplementary Table 1) for 1 h at room temperature. Nuclei were stained with Hoechst 33342. Confocal images were acquired using Olympus FluoVIEW FV 3000 and analyzed in Fiji.

Transmission Electron Microscopy

SC islets were fixed in 2.5% glutaraldehyde in 0.1 mol/L cacodylate buffer for 30 min at room temperature, post-fixed in reduced osmium, then stained with 0.5% uranyl acetate. After graded ethanol and acetone dehydration, samples were embedded in Epon resin and sectioned on a Leica UC7 ultramicrotome. Grids were examined with a Talos L120C G2 transmission electron microscope (TEM; Thermo Fisher Scientific) at 120 kV.

and WFS1$^{wt/757A>T}$ endocrine clusters. *G*: Violin plots detailing log-normalized UMIs of *CHGA* and pancreatic hormones (*INS*, *GCG*, *SST*, and *PPY*) in WFS1 and WFS1$^{wt/757A>T}$ endocrine clusters. *H*: Graphical representation of the relative percentage of both monohormonal (α-, β-, δ-, and PP) and polyhormonal cells in the endocrine clusters of WFS1 and WFS1$^{wt/757A>T}$ from scRNA-seq data. *I*: Violin plot detailing log-normalized UMIs of β-cell maturation markers in WFS and WFS1$^{wt/757A>T}$ endocrine clusters. *$P < 0.05$, **$P < 0.01$, ***$P < 0.001$ by Mann-Whitney nonparametric test.

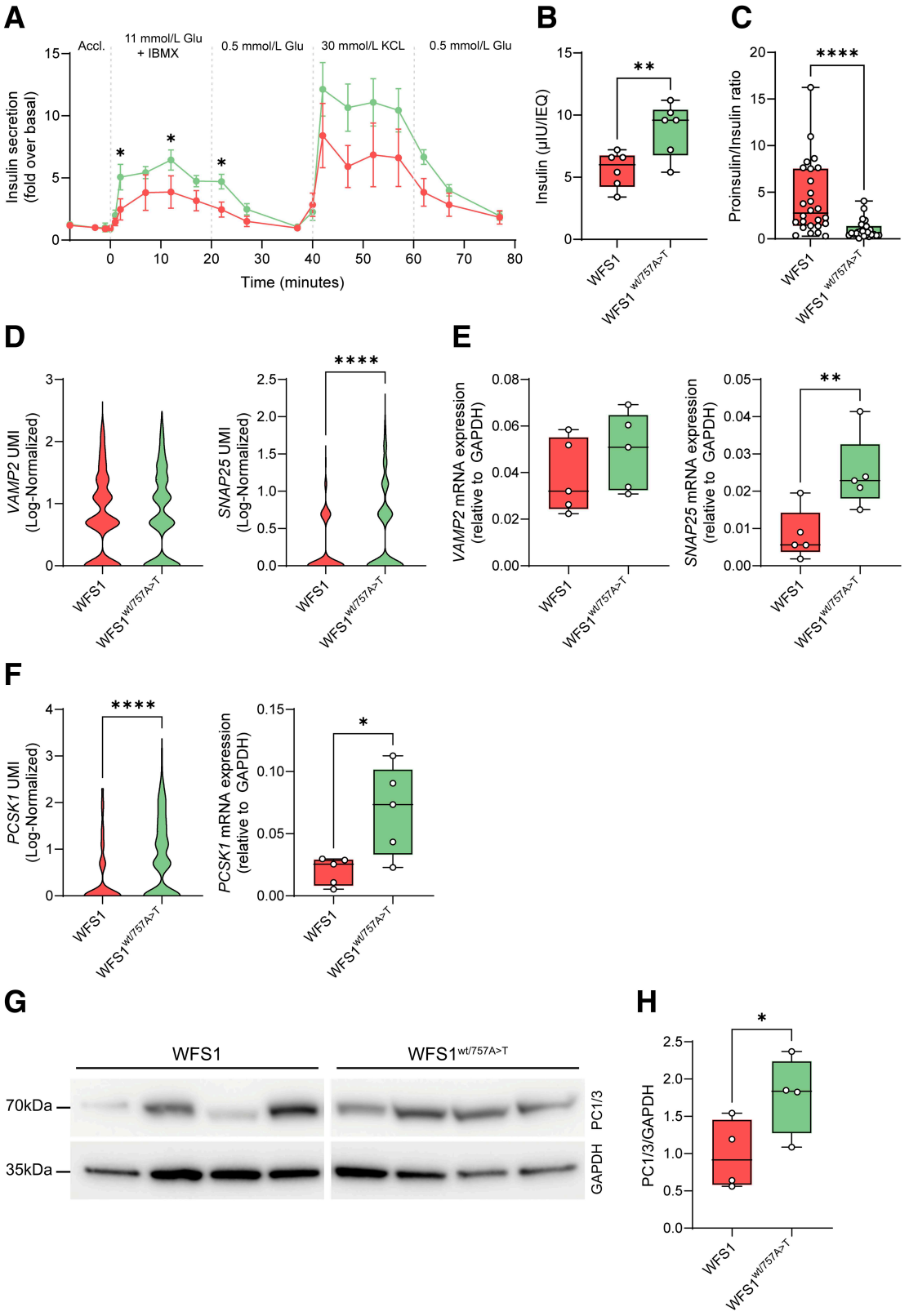

Figure 2—Wolframin alteration determines impaired insulin processing. *A*: Dynamic human insulin secretion expressed as fold change over $t = 0$ secretion in 0.5 mmol/L glucose ($n = 5$ for WFS1 and $n = 6$ for WFS1$^{wt/757A>T}$). *$P < 0.05$ by unpaired two-tailed t test. *B*: Insulin content expressed as international unit (IU) per islet equivalent (IEQ). Data are presented as mean ± SD ($n = 6$). **$P < 0.01$ by unpaired two-tailed t test. *C*: Proinsulin-to-insulin ratio quantification of insulin secreted when clusters were perfused with 11 mmol/L glucose + IBMX. Data are presented as mean ± SD ($n = 5$–6). ****$P < 0.0001$ by unpaired one-tailed t test. *D*: Violin plots reporting the log-normalized expression and expression levels measured by RT-qPCR of the SNARE complex-related *VAMP2* and *SNAP25* genes in the endocrine

RNA Extraction, Retrotranscription, and Quantitative RT-PCR

Total RNA was isolated with the mirVana Kit (Thermo Fisher), treated with TURBO DNase (Thermo Fisher), and reverse-transcribed using SuperScript IV (Invitrogen). Gene expression was profiled via TaqMan Array microfluidic cards (Applied Biosystems) containing 48 endocrine markers (Supplementary Table 2) or SYBR-based quantitative RT-PCR (RT-qPCR) (Supplementary Table 3) on a QuantStudio 12K Flex (Applied Biosystems). Results were normalized to GAPDH and reported as $2^{-\Delta Ct}$ or $2^{-\Delta\Delta Ct}$.

Single-Cell RNA Sequencing

WFS1 and WFS1$^{wt/757A>T}$ SC islets were dissociated and captured on the Chromium 10X platform (v3). Reads (~150 million/sample) were aligned to hg38 (GENCODE v31). Quality filtering removed cells with <200 or >7,000 genes, or >25% mitochondrial content. Data were analyzed in Seurat v4 (R v4.0.3), using variable gene selection, principal component analysis, Uniform Manifold Approximation and Projection, and shared nearest neighbor clustering (resolution, 0.5). Clusters were identified by comparing top cluster genes with existing single-cell pancreas atlases (21,22). Differentially expressed genes were selected with $\log_2$ fold change >1 and adjusted $P < 0.01$. Gene ontology enrichment analysis was performed directly from the home page of the Gene Ontology Consortium website (https://geneontology.org/).

Dynamic Perifusion and Insulin Content Analysis

For dynamic insulin secretion, 200 SC islet clusters were placed in a BioRep Perifusion system. Stimulation buffers contained 0.5 mmol/L glucose, then 11 mmol/L glucose ± 50 μmol/L 3-isobutyl-1-methylxanthine (IBMX), 11 mmol/L glucose ± 1 μmol/L liraglutide, or 30 mmol/L KCl. Perifusates were collected each minute, and insulin/proinsulin levels were measured by ELISA (Mercodia, RayBiotech). Results are shown as fold over basal secretion measured at the end of the acclimatization period at 0.5 mmol/L glucose. For insulin content measurement, 250 SC islet clusters were lysed in M-PER reagent (Thermo Fisher) and assayed by ELISA (Mercodia, RayBiotech). Insulin content was then expressed in international units per islet equivalent, where one islet equivalent corresponds to the volume of a standard islet of ~150 μm in diameter, thus normalizing for variations in islet size.

Ca^{2+} Flux Assay

SC islet clusters were plated on Matrigel-coated optical plates (Greiner) for 2–3 days. Cells were loaded with 1 μmol/L Fluo-4 AM (Invitrogen) in HEPES-buffered solution, and then imaged every 2 s on a Zeiss Axio Observer.Z1. After 1 min, secretagogues were added, and fluorescence changes were recorded for up to 300 s. Signals from 10 cells in each of two different in vitro differentiation protocols (for a total of 20 cells) were processed in Fiji, MATLAB, and R software to quantify oscillation amplitude, period, plateau fraction, and coactivity, as previously described (23,24).

Western Blot

Protein lysates were prepared in M-PER reagent (Thermo Fisher) or a buffer containing 65 mmol/L Tris, pH 6.8, 4% SDS, 1.5% β-mercaptoethanol, and protease/phosphatase inhibitors. Samples were quantified (Pierce BCA), separated by SDS-PAGE, and transferred to polyvinylidene fluoride membranes. Blots were blocked in Tris-buffered saline with 0.1% Tween 20 and 5% milk or BSA, and incubated overnight at 4°C with primary antibodies (Supplementary Table 1), followed by horseradish peroxidase-conjugated secondaries. Bands were visualized using SuperSignal West Pico PLUS (Thermo Fisher) and quantified in Fiji.

Statistical Analysis

Analyses were performed in GraphPad Prism 9.0.1 software. Two-group comparisons used unpaired or paired Student *t* tests or Mann-Whitney tests. Multiple comparisons were assessed by one-way or two-way ANOVA with the Dunn-Šídák correction. Significance was set at $P < 0.05$. Data are shown as mean ± SD unless otherwise stated, with details on statistical tests provided in figure legends.

Data and Resource Availability

Raw data from the single-cell RNA sequencing (scRNA-seq) experiment have been submitted and are awaiting publication in the Gene Expression Omnibus database under BioProject PRJNA1109747. Any additional raw data not directly included in this manuscript or deposited in an online repository are available from the corresponding authors upon request.

RESULTS

WFS1 iPSCs Efficiently Differentiate In Vitro Into the Pancreatic Lineage but Show Less Mature Endocrine Phenotype and Impaired Insulin Secretion

In our previous study, we generated patient-derived iPSCs (WFS1) and the isogenic line in which the c.316-1G>A mutation was genetically corrected (WFS1$^{wt/757A>T}$), restoring the wild-type isoform of wolframin (20) (Fig. 1*A*).

clusters of WFS1 and WFS1$^{wt/757A>T}$ SC islets. ****$P < 0.0001$ by Mann-Whitney nonparametric test. *E*: The expression levels measured by RT-qPCR of *SNAP25* and *VAMP2* genes in WFS1 and WFS1$^{wt/757A>T}$ SC islets ($n = 5$). **$P < 0.01$ by unpaired two-tailed *t* test. *F*: Log-normalized expression of *PCSK1* gene in the endocrine clusters from scRNA-seq experiment and analysis of its expression levels by RT-qPCR in WFS1 and WFS1$^{wt/757A>T}$ SC islets ($n = 5$). ****$P < 0.0001$ by Mann-Whitney nonparametric test for scRNA-seq; and *$P < 0.05$ by unpaired two-tailed *t* test for RT-qPCR. *G*: Immunoblot analysis of PC1/3 expression in WFS1 and WFS1$^{wt/757A>T}$ SC islets. *H*: Relative quantification of PC1/3 to GAPDH (housekeeping) expression in WFS1 and WFS1$^{wt/757A>T}$ SC islets ($n = 4$). *$P < 0.05$ by unpaired one-tailed *t* test.

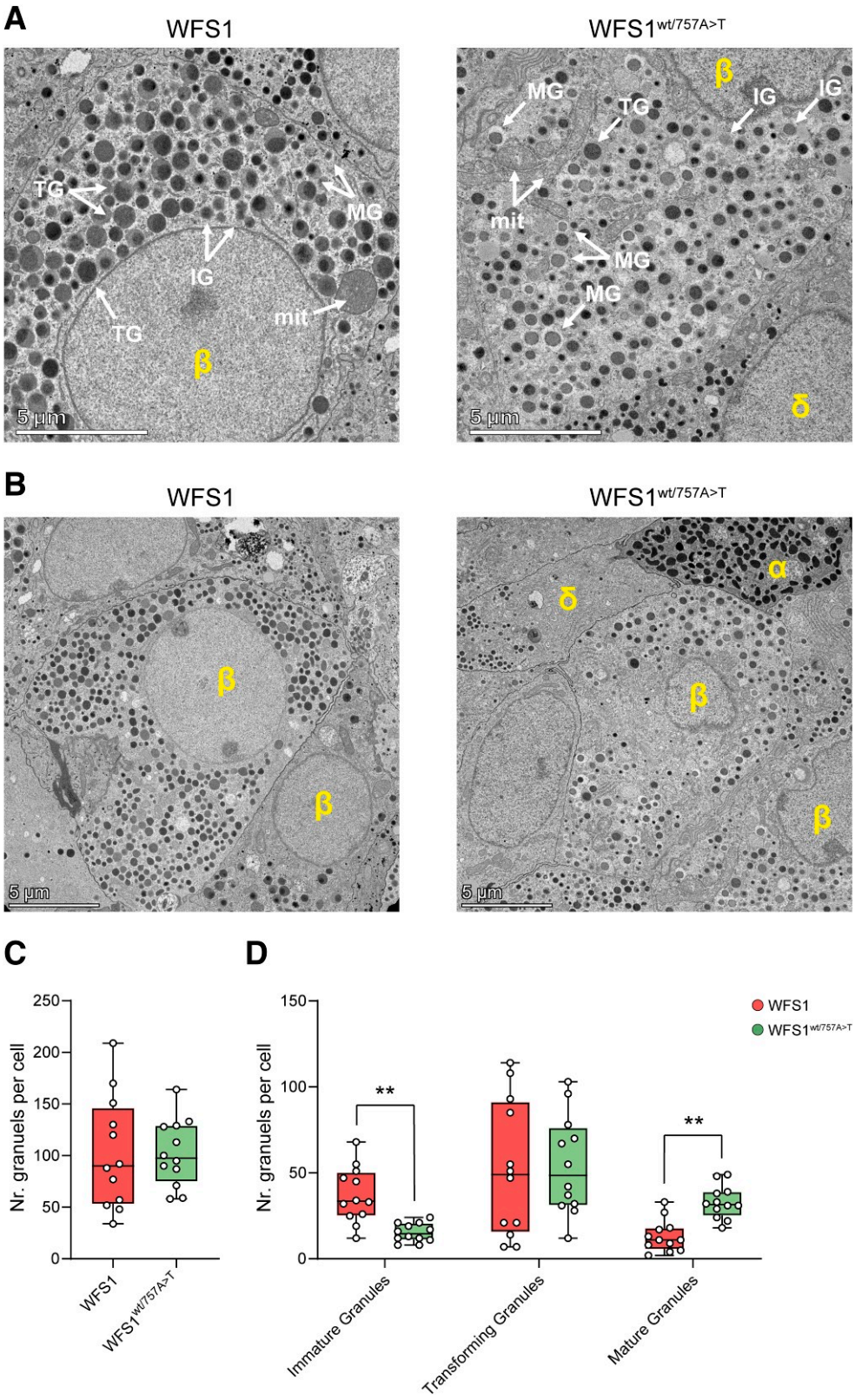

Figure 3—WFS1 SC islets show morphological defects in secretory granule maturation. *A*: TEM images of sections from WFS1 and WFS1$^{wt/757A>T}$ SC islets indicating morphologies of mature secretory granules (MG), immature secretory granules (IG), and transforming secretory granules (TGs). MGs contain a dark core of condensed insulin surrounded by a large halo; IGs are located near the Golgi network and have no halo; TGs are close to the nucleus or mitochondria (mit) and have a narrow halo. *B*: TEM images showing the insulin secretory granules in WFS1 and WFS1$^{wt/757A>T}$ SC islets. The different cell types (α, β, and δ) are also highlighted. Scale bar is 5 μm. Quantification of the total number (*C*) and IGs, TGs, and MGs (*D*) per cell in WFS1 and WFS1$^{wt/757A>T}$ SC islets ($n = 12$). $^{**}P < 0.01$ by unpaired two-tailed *t* test.

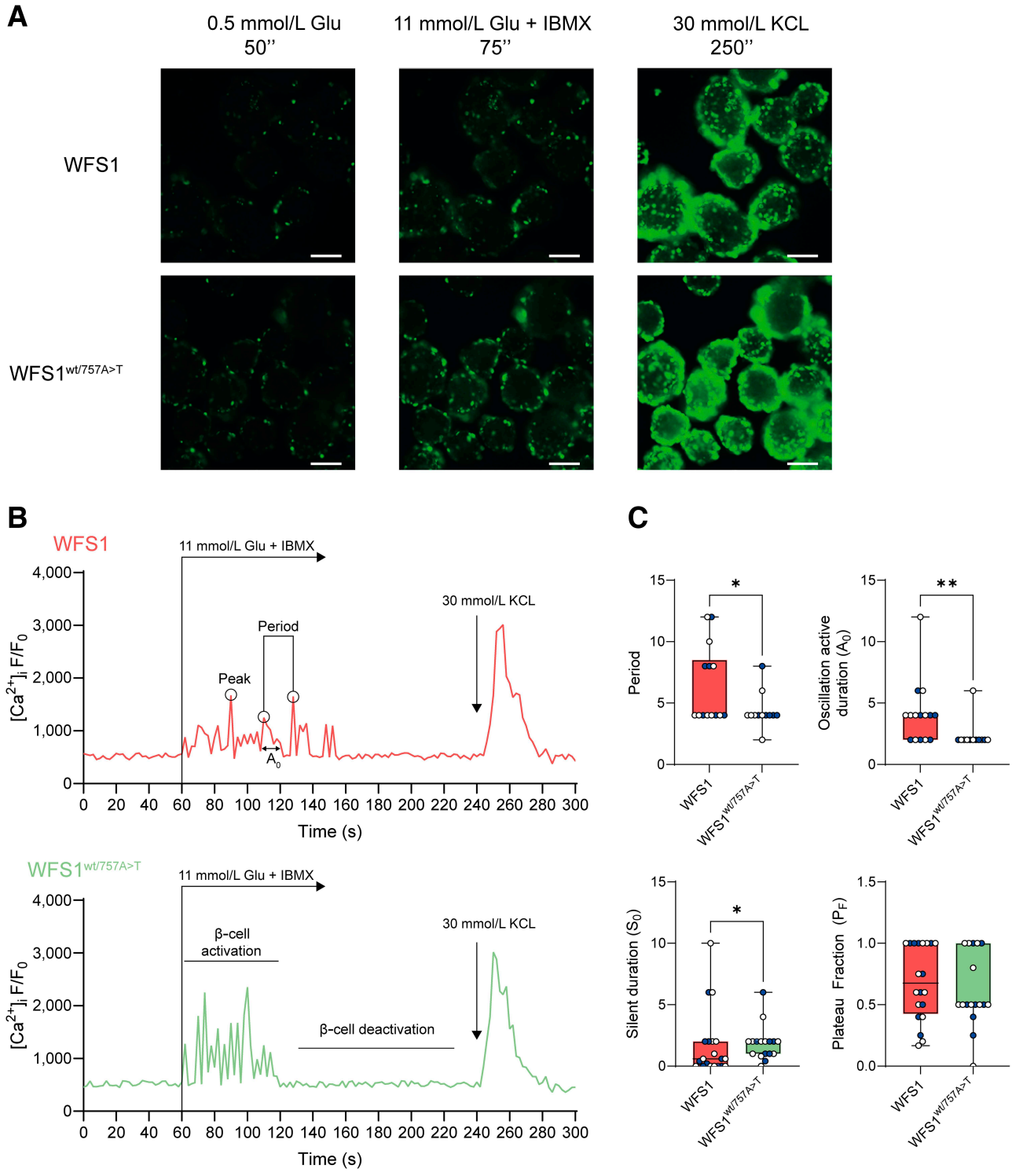

Figure 4—Calcium flux dynamics is altered in WFS1 SC islets. *A*: Imaging of calcium flux using Fluo-4 dye in WFS1 and WFS1$^{wt/757A>T}$ SC islets after 50-, 75-, and 250-s stimulation with 0.5 mmol/L glucose (Glu), 11 mmol/L glucose supplemented with IBMX, and 30 mmol/L KCl, respectively. Objective magnification: ×10. *B*: Mean fluorescence signal (F/F_0) over time in WFS1 and WFS1$^{wt/757A>T}$ SC islets indicating $[Ca^{2+}]_i$ elevation in response to stimulation with 11 mmol/L glucose + IBMX. Peak (the maximum value of each oscillation), period (the length of time between two peaks), and active duration (A_0, the length of time for Ca^{2+} oscillation measured at half of the peak height) are indicated within the WFS1 graph. The timing of β-cell activation and deactivation are highlighted in the WFS1$^{wt/757A>T}$ graph (n = 20-). *C*: Mean period upon stimulation, active and silent duration of oscillation, and plateau fraction measured in WFS1 and WFS1$^{wt/757A>T}$ β-cells (n = 20 cells from two different in vitro differentiation protocols, represented by white and blue circles, respectively). *$P < 0.05$, **$P < 0.01$ by Mann-Whitney nonparametric test.

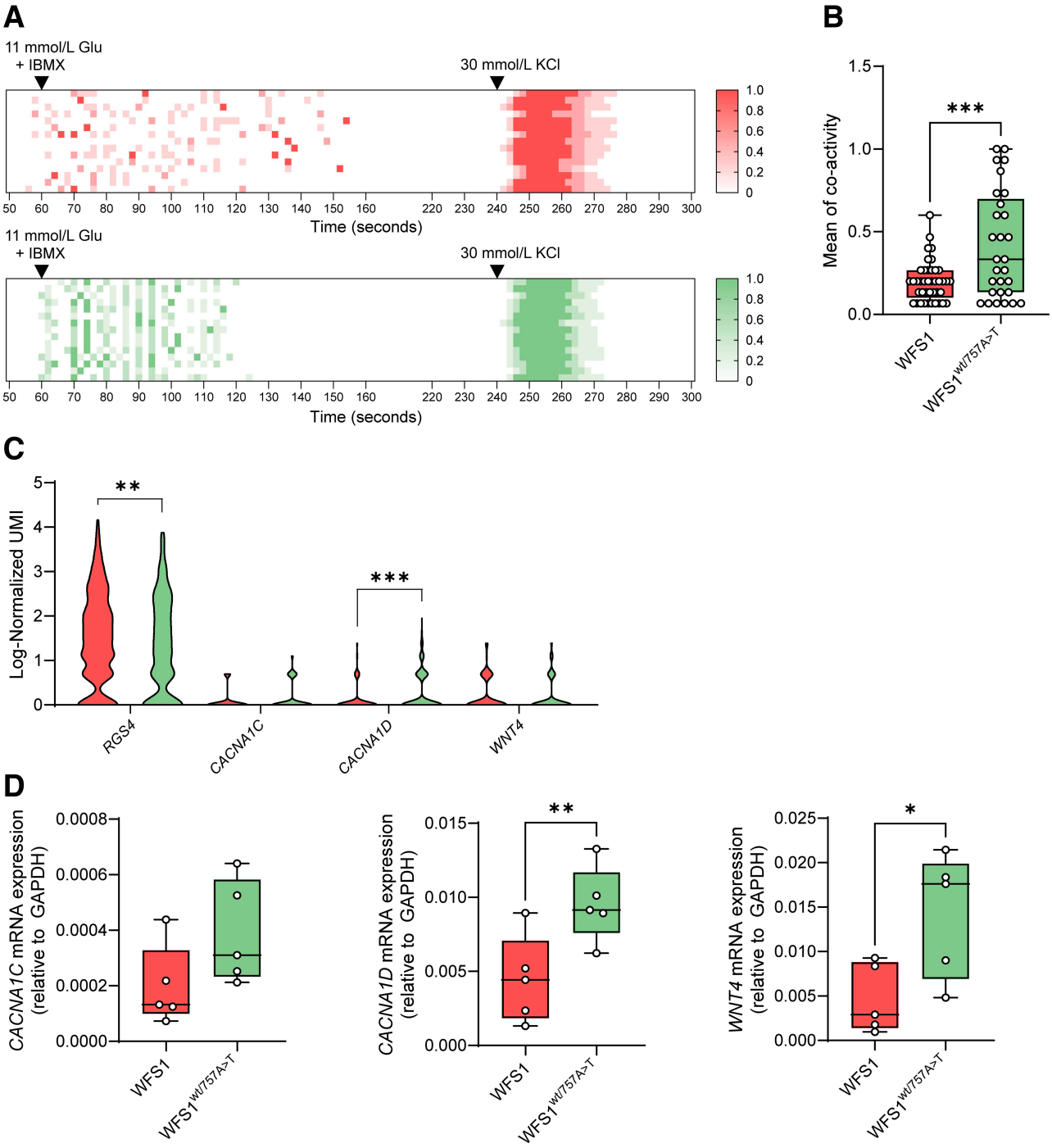

Figure 5—Dysregulation of the insulin secretory machinery in WFS1 SC islets. *A*: Graphical representation of calcium oscillations in 15 WFS1 or WFS1$^{wt/757A>T}$ cells after stimulation with 11 mmol/L glucose (Glu) supplemented with IBMX, followed by 30 mmol/L KCl. *B*: Mean coactivity coefficient in WFS1 or WFS1$^{wt/757A>T}$ cells stimulated with 11 mmol/L glucose supplemented with IBMX ($n = 20$). ***$P <$ 0.001 by unpaired two-tailed *t* test. *C*: Violin plot reporting the log-normalized expression of the calcium-related genes *RGS4*, *CACNA1C*, *CACNA1D*, and *WNT4* in the endocrine clusters of WFS1 and WFS1$^{wt/757A>T}$ SC islets. **$P < 0.01$, ***$P < 0.001$ by Mann-Whitney non-parametric test. *D*: Expression levels measured by RT-qPCR of *CACNA1C-D* and *WNT4* genes in WFS1 and WFS1$^{wt/757A>T}$ SC islets ($n = 5$). *$P < 0.05$, **$P < 0.01$ by unpaired two-tailed *t* test.

WFS1 and WFS1$^{wt/757A>T}$ iPSCs were terminally differentiated into SC-derived islets (Fig. 1*B*) to evaluate the impact of *WFS1* mutations on differentiation efficiency. However, the expression of PDX1 at the pancreatic progenitor stage and of NKX6-1 and insulin at the end of differentiation revealed no evident defects in the pancreatic differentiation capacity of WFS1 cells compared with their genetically corrected counterparts (20) (Fig. 1*C* and *D*). These data were confirmed by the expression of genes involved in pancreatic development, production of hormones

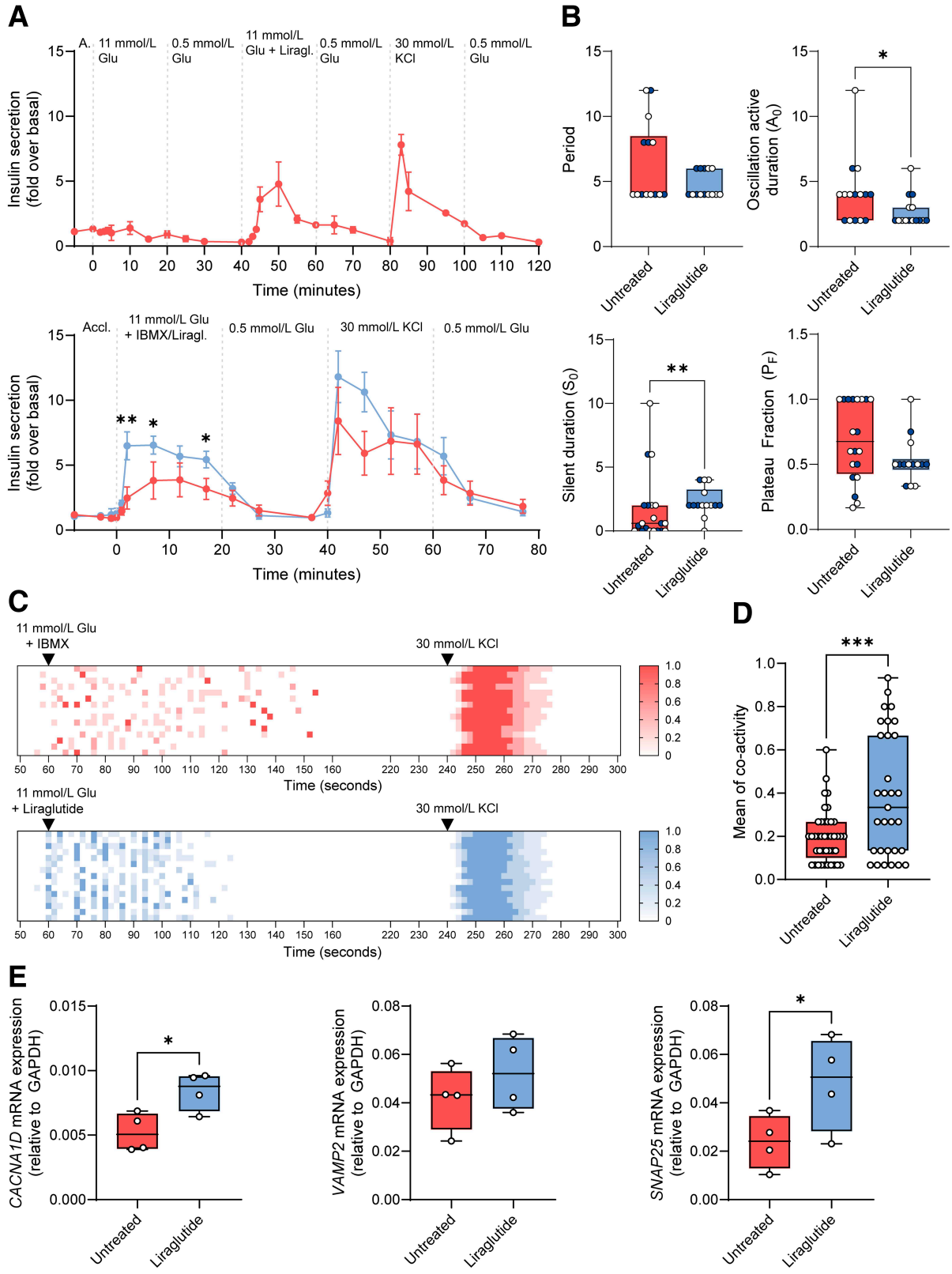

Figure 6—Liraglutide restores calcium flux and secretory impairments. *A*: (Top) Dynamic insulin secretion expressed as fold change over basal secretion of WFS1 SC islets stimulated with 11 mmol/L glucose, followed by an additional stimulation with 11 mmol/L glucose supplemented with 1 μmol/L liraglutide or (bottom) stimulated with 11 mmol/L glucose supplemented with IBMX (red) or liraglutide (blue) ($n = 5$). *$P < 0.05$, **$P < 0.01$ by unpaired two-tailed *t* test. *B*: Mean period (length of time between two peaks), active (length of time for each Ca^{2+} oscillation measured at half of the peak height, referred to as active duration), and silent duration (electrically silent "triggering" phase, which culminates in membrane depolarization) of oscillations, plateau fraction (which measures the proportion of time spent in active phase over a

and autoantigens of β-cells, and insulin secretion and glucose sensing (Supplementary Fig. 1*A*).

To deeply investigate the endocrine compartment, we performed scRNA-seq analysis on 4,594 WFS1 cells and 2,215 and WFS1$^{wt/757A>T}$ cells from SC islets (Supplementary Fig. 1*B*–*G*). The unsupervised clustering uncovered seven subpopulations, based on the top upregulated genes (Supplementary Fig. 1*H* and *I* and Fig. 1*E*) (25). Although the downregulation of the *WFS1* gene in WFS1 SC islets was expected (20) (Fig. 1*F*), interestingly, we found significantly higher expression of *INS* (5.92 ± 0.88 vs. 3.90 ± 1.13; $P < 0.001$) in these cells compared with WFS1$^{wt/757A>T}$, but a slight reduction of *CHGA* (4.48 ± 0.90 vs. 4.89 ± 1.02; $P < 0.01$) and *PPY* (0.80 ± 1.21 vs. 1.97 ± 1.18; $P < 0.01$) (Fig. 1*G*). While the average expression levels of *GCG* and *SST* were comparable (Fig. 1*G*), there was a consistent difference between the subpopulations within the endocrine compartments. Indeed, WFS1 SC islets had a greater proportion of β-cells, but significantly lower mature α-cells, δ-cells, and pancreatic polypeptide cells than WFS1$^{wt/757A>T}$ (Fig. 1*H*). Moreover, WFS1 cells displayed significantly higher levels of the early endocrine markers *MAFB* and *ISL1*, but reduced expression of *NEUROD1*, *NKX2-2*, *NKX6-1*, and *FEV* than WFS1$^{wt/757A>T}$, and WFS1 endocrine cells showed a FEV-to-ISL1 ratio ≈1, whereas it was >2 in WFS1$^{wt/757A>T}$ (Fig. 1*I*). Consistent with the evidence that the onset of FEV preceding ISL1 initiation is indicative of α-/β-cell fate and, vice versa, the expression of ISL1 over FEV predicts an immature, polyhormonal profile (25), we found reduced expression of *MNX1* in WFS1 SC islets (0.37 ± 0.57 vs. 1.21 ± 0.87; $P < 0.001$), a transcription factor pivotal for β-cell–like maturation (Fig. 1*I*). Moreover, we observed high frequency of INS$^+$/GCG$^+$/SST$^+$ or INS$^+$/GCG$^+$/PPY$^+$ polyhormonal cells in WFS1 (12.2%) compared with WFS1$^{wt/757A>T}$ (6.4%) SC islets (Fig. 1*H*). Further evaluation of the differentially expressed late β-cell markers *UCN3*, *SYT4*, *CFAP126*, and *MAFA* supported the hypothesis that WFS1 SC islets displayed a less mature phenotype than their gene-edited counterpart (Fig. 1*I* and Supplementary Fig. 2*A*). Of note, biological pathway analysis of scRNA-seq data revealed alterations in the secretory machinery, calcium-related activities, insulin signaling, and inflammatory response (Supplementary Fig. 2*B*–*D*).

We then investigated how the immature phenotype influenced glucose responsiveness, revealing a pronounced defect encompassing both insulin secretory capacity and total insulin amount in WFS1 SC islets (Fig. 2*A* and *B* and Supplementary Fig. 3*A*). Interestingly, the proinsulin-to-insulin ratio upon high glucose stimulation was altered in WFS1 cells compared with WFS1$^{wt/757A>T}$ (4.12 ± 0.95 vs. 0.69 ± 0.14; $P < 0.01$), suggesting a disruption in the normal processing of insulin in mutant cells, underlying β-cell stress or damage (Fig. 2*C*).

WFS1 SC Islets Display Dysregulated Insulin Secretion Machinery and Altered Ca^{2+} Dynamics

As the exocytosis of insulin-containing granules in pancreatic β-cells is essential to their function, we investigated the pathways involved in the priming and fusion of secretory granules with plasma membrane preceding their Ca^{2+}-dependent exocytosis and consequent insulin release (26). The transcriptional levels of the synaptosomal-protein of 25 kD (SNAP25) interacting with the vesicle-associated membrane protein 2 (VAMP2) were significantly reduced in WFS1 SC islets compared with the gene-edited counterpart (Fig. 2*D* and *E*), supporting a defect of the secretory machinery. We also observed a reduction of *PCSK1* gene expression (Fig. 2*F*) and its protein product PC1/3 (Fig. 2*G* and *H*) in WFS1 SC islets compared with WFS1$^{wt/757A>T}$, indicating impaired insulin processing. These data were consistent with the morphology of secretory granules (27) (Fig. 3*A* and *B*). Indeed, while there is no difference in the total number of insulin granules, they appeared more immature in WFS1 β-cells than in their genetically corrected counterparts (Fig. 3*C* and *D*).

To deeply understand the mechanisms driving the impairment of insulin secretion in WFS1 SC islets, we measured the Ca^{2+} dynamics in response to high glucose stimulation or high glucose supplemented with IBMX. While Ca^{2+} concentrations oscillated synchronously in WFS1$^{wt/757A>T}$ SC islets, they did not propagate simultaneously through the cells in WFS1 SC islets, which appeared also affected by delayed β deactivation (Supplementary Fig. 3*B* and Fig. 4*A* and *B*). Indeed, Ca^{2+} oscillations changed their average peak during the transition from low to high glucose concentrations and increased their period and time in the active phase in WFS1 SC islets compared with their WFS1$^{wt/757A>T}$ counterpart (Fig. 4*C*). Conversely, the silent duration was reduced in WFS1 SC islets, while the plateau fraction did not show significant differences between the genotypes (Fig. 4*C*). The analysis of Ca^{2+} oscillations after high glucose plus IBMX stimulation and the mean of coactivity supported the evidence of asynchronous waves in WFS1 compared with WFS1$^{wt/757A>T}$ SC islets (Fig. 5*A* and *B*).

We then examined the expression of *RGS4*, encoding for the regulator of G protein signaling 4, a negative regulator of insulin secretion in pancreatic β-cells (28), and *CACNA1C* and *CACNA1D* genes, coding for calcium voltage-gated channel subunit alpha1 C (CACNA1C) and D (CACNA1D), respectively. The scRNA-seq revealed *RGS4* upregulation

single period) in WFS1 β-cells following 11 mmol/L glucose stimulation, without or with 1 μmol/L liraglutide ($n = 20$ from two different in vitro differentiation protocols, represented by white and blue circles, respectively). *$P < 0.05$, **$P < 0.01$ by Mann-Whitney nonparametric test. *C*: Graphical representation of calcium oscillations in 15 WFS1 β-cells after stimulation with 11 mmol/L glucose supplemented with IBMX or liraglutide, followed by 30 mmol/L KCl. *D*: Mean coactivity coefficient (number of cells with similar peak profiles; $n = 20$). ***$P < 0.001$ by unpaired two-tailed *t* test. *E*: RT-qPCR analysis of the expression levels of *CACNA1D* and the SNARE complex-related genes *SNAP25* and *VAMP2* in WFS1 SC islets treated or not with 1 μmol/L liraglutide ($n = 4$). *$P < 0.05$ by unpaired one-tailed *t* test.

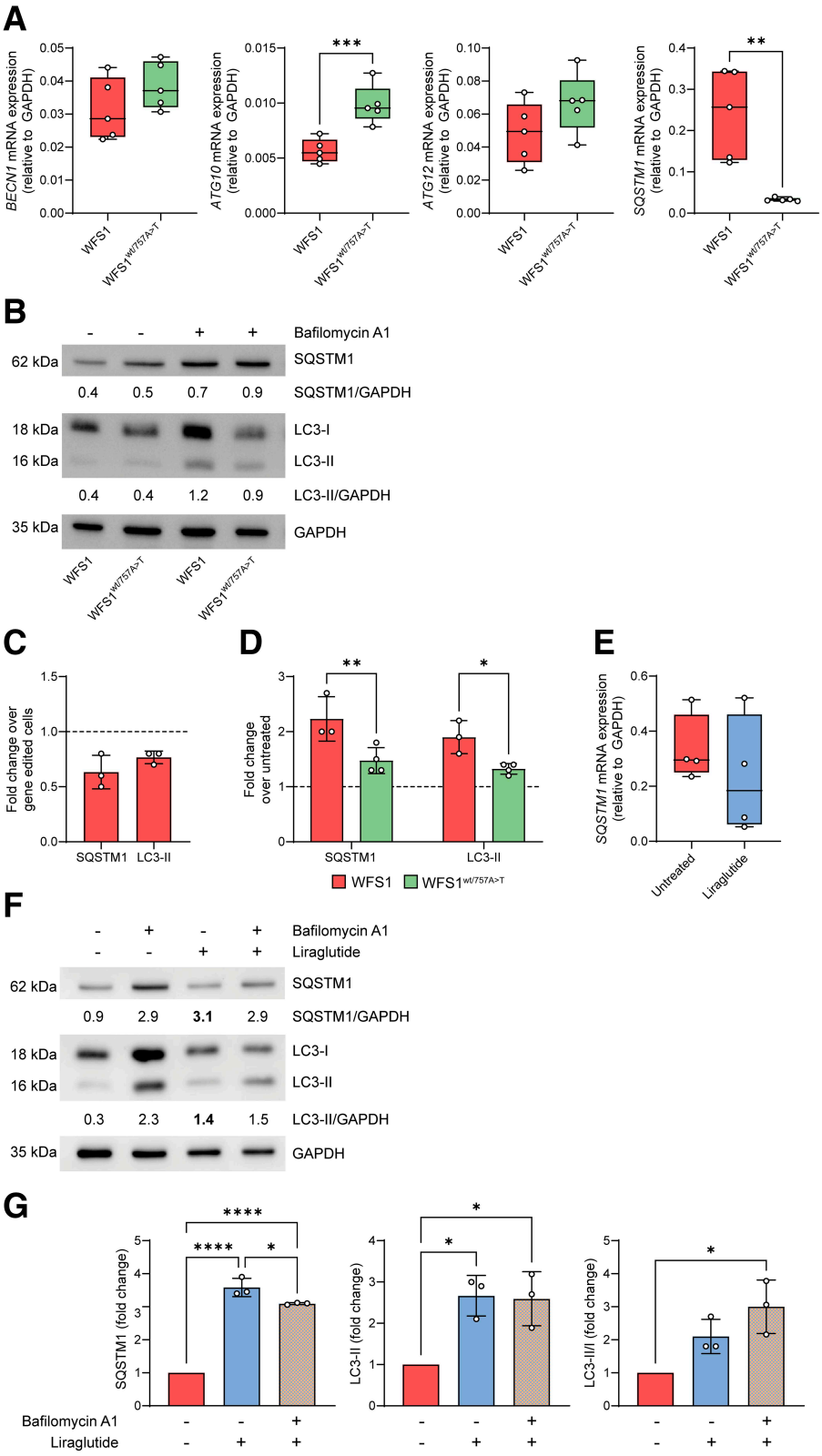

Figure 7—Abnormal autophagy is restored by liraglutide. *A*: Expression levels measured by RT-qPCR of *BECN1*, *ATG10*, *ATG12*, and *SQSTM1* genes in WFS1 and WFS1$^{wt/757A>T}$ SC islets. GAPDH was used as housekeeping ($n = 5$). $^{**}P < 0.01$, $^{***}P < 0.001$ by unpaired two-tailed *t* test. *B*: Representative immunoblot for analysis of SQSTM1 and LC3-II in WFS1 and WFS1$^{wt/757A>T}$ SC islets treated or not with 100 nmol/L bafilomycin A1 for 2 h. *C*: Levels of SQSTM1 and LC3-II normalized to GAPDH in WFS1 SC islets expressed as fold change over WFS1$^{wt/757A>T}$ SC islets. Data are reported as mean ± SD ($n = 3$). *D*: Levels of SQSTM1 and LC3-II normalized to GAPDH in WFS1 and WFS1$^{wt/757A>T}$ SC islets 2 h after 100 nmol/L bafilomycin treatment expressed as fold change over untreated cells. Data are reported as mean ± SD ($n = 3$). $^{*}P < 0.05$, $^{**}P < 0.01$ by paired two-tailed *t* test. *E*: RT-qPCR analysis of the expression levels of *SQSTM1* in

(1.50 ± 1.02 in WFS1 vs. 1.32 ± 1.06 in WFS1$^{wt/757A>T}$; $P < \psi 0.01$) and concomitant *CACNA1D* decrease (0.10 ± 0.28 in WFS1 vs. 0.27 ± 0.44 in WFS1$^{wt/757A>T}$; $P < \psi 0.001$) (Fig. 5*C*) in WFS1 SC islets, indicating a strong inhibition of calcium release at least partly due to an impairment of Ca^{2+} channels. RT-qPCR analysis confirmed a statistically significant decrease of *CACNA1D* mRNA (Fig. 5*D*), suggesting that CACNA1D is relevant for insulin secretion in WS1. Moreover, WFS1 SC islets showed more than twofold lower levels of *WNT4* compared with their corrected counterparts (0.004 ± 0.0038 vs. 0.014 ± 0.007; $P < \psi 0.05$). WNT4 controls Ca^{2+} signaling in response to glucose challenge (29), suggesting that the Wnt pathway is affected in WS1 and may contribute to impairments in glucose-stimulated insulin secretion (GSIS) (Fig. 5*D*).

All together, these results highlight the dysregulation of several β-cell–specific pathways, ultimately leading to impaired β-cell function in WS1.

The GLP-1R Agonist Liraglutide Restores the Ca^{2+} Oscillation and Secretory Impairments, Increasing Glucose Responsiveness and Insulin Release

Finally, we investigated whether the mechanisms we found dysregulated in patient-derived WFS1 SC islets might be positively impacted by liraglutide treatment and, therefore, whether their targeting might account for the efficacy of liraglutide in this patient (17). We first inspected the effect of acute liraglutide treatment on glucose responsiveness and insulin secretion in WFS1 SC islets. Liraglutide increased insulin secretion after a second stimulation with high glucose concentration compared with the first stimulation with high glucose alone. The same effect (twofold increase) was observed when liraglutide was used in combination with high glucose and IBMX stimulation (Fig. 6*A*) or high glucose alone (Supplementary Fig. 4*A*) in comparison with untreated cells. Indeed, while the period did not significantly changed between the two experimental groups, the active phase of oscillations was lower in liraglutide-treated SC islets (2.66 ± 1.17 vs. 4.13 ± 2.55; $P < \psi 0.05$), and consistently, the silent period of oscillations significantly increased (2.28 ± 1.13 vs. 1.67 ± 2.66; $P < \psi 0.01$) (Fig. 6*B*). Accordingly, the mean of coactivity rose to 67% after liraglutide exposure compared with untreated cells (Fig. 6*C* and *D*). Interestingly, the acute administration of liraglutide ameliorated average peak and Ca^{2+} oscillations in both WFS1 and WFS1$^{wt/757A>T}$ SC islets treated with 50 nmol/L thapsigargin (TG) for 8 h to induce sustained activation of ER stress (Supplementary Fig. 4*B–D*), supporting the hypothesis that GLP-1R agonists can actively counteract cellular stress-dependent impairments. Moreover, liraglutide restored the defects of the exocytosis machinery as well as the calcium voltage-gated channels as demonstrated by increased transcription of both *SNAP25* (0.048 ± 0.019 vs. 0.023 ± 0.011; $P < \psi 0.05$) and *CACNA1D* (0.0083 ± 0.0014 vs. 0.0052 ± 0.0014; $P < \psi 0.05$). Of note, the drug did not have any significant impact on *VAMP2* (Fig. 6*E*).

WFS1 SC Islets Show Enhanced Autophagic Flux Under Basal Conditions

The loss of wolframin has been reported to disrupt Ca^{2+} dynamics, triggering the activation of autophagy and mitophagy (30,31). To give a deeper insight into the mechanisms responsible for reduced insulin secretion in WFS1 SC islets, we first analyzed the transcription levels of the key regulators *ATG10*, *ATG12*, and *BECN1* participating in autophagosome formation, but we did not find statistically significant differences between WFS1 SC islets and their corrected counterpart, except for significantly reduced *ATG10* transcripts in WFS1 SC islets (0.0056 ± 0.0010 vs. 0.0098 ± 0.0017). Surprisingly, the autophagy substrate *SQSTM1* mRNA was strongly upregulated in WFS1 compared with WFS1$^{wt/757A>T}$ SC islets (0.24 ± 0.10 vs. 0.033 ± 0.004; $P < \psi$ 0.01) (Fig. 7*A*). Moreover, patient-derived SC islets showed reduced LC3-II and SQSTM1 expression levels compared with their corrected counterparts (Fig. 7*B* and *C*), suggesting that enhanced autophagic degradation occurs in WFS1 SC islets. We further explored the autophagic flux by treating SC islets with bafilomycin A1, which inhibits autophagic degradation blocking the endolysosomal acidification. We observed increased levels of LC3-II in bafilomycin-treated WFS1$^{wt/757A>T}$, which was even higher in WFS1 SC islets. Consequently, SQSTM1 protein levels were higher in WFS1 SC islets compared with their corrected counterpart, suggesting that *WFS1* mutation enhanced the autophagic flux (Fig. 7*B* and *D*). These results are indeed concordant with the increase of *SQSTM1* transcripts (Fig. 7*A*), which constitutes an attempt at restoring SQSTM1 protein levels in basal conditions. We then explored the potential impact of liraglutide on the autophagic pathway in WFS1 SC islets and found that the GLP-1R agonist increased LC3-II and the LC3-II–to–LC3-I ratio, suggesting autophagy induction, and boosted protein level of SQSTM1 without significant changes in its transcripts, probably caused by transient accumulation due to enhanced autophagosome formation (Fig. 7*E–G*).

Chronic Liraglutide Exposure Protects WFS1 SC Islets From Thapsigargin and Proinflammatory Cytokines-Induced Apoptosis

We demonstrated that patient-derived SC islets are susceptible to cellular stress and proinflammatory cytokines-induced cell death (20). Strikingly, both early and late

WFS1 SC islets before and after treatment with 1 μmol/L liraglutide ($n = 4$). *$P < 0.05$ by unpaired one-tailed *t* test. *F*: Representative immunoblot for analysis of SQSTM1 and LC3-II in WFS1 SC islets treated or not with 100 nmol/L bafilomycin A1 and/or 1 μmol/L liraglutide for 2 h. *G*: SQSTM1 and LC3-II levels normalized to GAPDH and the LC3-II/I ratio in WFS1 after liraglutide and/or bafilomycin A1 treatment are presented as fold changes relative to untreated WFS1 SC islets. Data are reported as mean ± SD ($n = 3$). *$P < 0.05$, ****$P < 0.0001$.

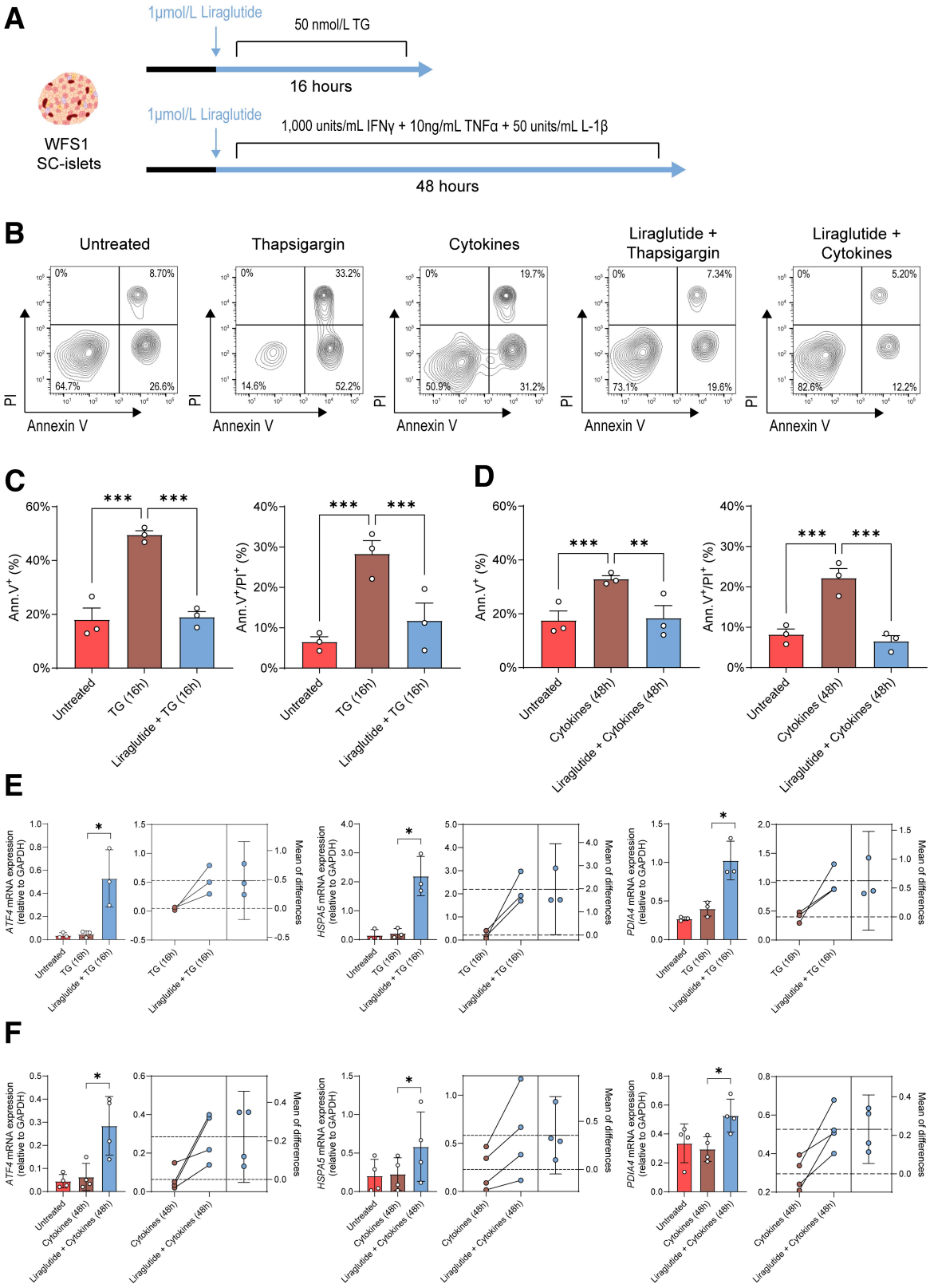

Figure 8—Liraglutide protects from stress and inflammation-induced apoptosis. *A*: Schematic summary of chronic treatment with 1 µmol/L liraglutide in WFS1 SC islets exposed either to TG for 16 h or to inflammatory cytokines (interferon [IFN]-γ, tumor necrosis factor [TNF]-α and interleukin [IL]-1β) for 48 h. *B*: Representative FACS plots for analysis of annexin V (Ann.V) and propidium iodide (PI)-stained WFS1 cells after treatment with TG or cytokines, in presence or not of liraglutide. Early and late apoptosis was measured as the percentage (%) of Ann.V and PI-positive cells, respectively, in WFS1 SC islets after exposure to TG (*C*) or cytokines (*D*), with or without chronic treatment with liraglutide. Data are expressed as mean ± SD (n = 3). $^{**}P < 0.01$, $^{***}P < 0.001$ by two-way ANOVA with the Dunn-Šídák

apoptosis were prevented in liraglutide-treated SC islets exposed to TG or proinflammatory cytokines (Fig. 8*A*), as the percentage of annexin V^+ and propidium iodide-positive cells were comparable to the untreated and more than twofold lower than WFS1 SC islets exposed to stressors (Fig. 8*B–D*). The ability of liraglutide to mitigate apoptosis correlated with enhanced UPR. Indeed, we observed differences in basal and TG-stimulated unfolded protein response activation between WFS1 and $WFS1^{wt/757A>T}$ SC islets (Supplementary Fig. 5). By evaluating the expression changes of ER stress-related markers, we found a significant increase of *ATF4* (mean difference 0.48 ± 0.27; $P < 0.05$), *HSPA5* (mean difference 1.92 ± 0.79; $P < 0.05$), and *PDIA4* (mean difference 0.62 ± 0.34; $P < 0.05$) in WFS1 cells exposed to liraglutide and TG (Fig. 8*E*), and of *ATF4* (mean difference 0.22 ± 0.14; $P < 0.05$), *HSPA5* (mean difference 0.35 ± 0.25; $P < 0.05$), and *PDIA4* (mean difference 0.23 ± 0.11; $P < 0.05$) in WFS1 cells exposed to liraglutide and proinflammatory cytokines (Fig. 8*F*).

DISCUSSION

Wolframin contributes to several processes orchestrated by the ER, where it exerts its functions as a transmembrane protein. Wolframin modulates ER stress responses, regulates intracellular Ca^{2+} homeostasis, and acts at mitochondria-associated ER membranes in different tissues (2–6). Given its involvement in several cellular pathways, pathogenic variants in the *WFS1* gene are expected to affect cell survival and function as missense, nonsense, and frameshift mutations produce variable RNA and protein defects (32) and account for the broad spectrum of WS1 clinical manifestations.

In this study, we reported the alterations of cellular processes involved in endocrine function and survival of pancreatic β-cells in a WS1 patient harboring the c.316-1G>A mutation, generating two PTC-containing transcripts undergoing nonsense-mediated decay, as well as two open reading frame–conserving mRNAs that yield a partially functional wolframin (20). These atypical transcripts contributed to an unconventional cellular response to ER stress, prompting an in-depth characterization of β-cell differentiation and functionality.

Our data indicate that the *WFS1* mutation determines an overall immature endocrine phenotype as revealed by the presence of high levels of early endocrine markers and the enrichment of $INS^+/GCG^+/SST^+$ or $INS^+/GCG^+/PPY^+$ polyhormonal cells in patient-derived SC islets. While the percentage of INS^+ cells was relatively high, their maturation was compromised compared with $WFS1^{wt/757A>T}$ SC islets, which exhibited higher transcription levels of the mature β-cell function gene signature. The morphology of insulin secretory granules supported a defect in their maturation processing as WFS1 β-cells exhibit more immature granules compared with the gene-edited counterparts.

The immature endocrine phenotype reflected in impaired GSIS and was associated with enrichment gene ontology terms related to insulin signaling, secretory machinery, calcium-related activities, and inflammatory response. Indeed, lower expression of *SYT4*, *CFAP126*, and *WNT4* in WFS1 SC islets likely contributed to dysregulated Ca^{2+} fluxes and GSIS (33–35). Moreover, SNAP25, a pivotal SNARE complex component for insulin exocytosis (36), was markedly reduced in WFS1 SC islets. Since SNAP25 is important for synchronized Ca^{2+} oscillations and robust insulin release (37), its downregulation, along with decreased *CACNA1D* (Cav1.3 channels) and *WNT4*, and increased *RGS4*, further explains the reduced insulin response and asynchronous Ca^{2+} flux (38,39). Additionally, diminished PC1/3 correlated with an increased proinsulin-to-insulin ratio, reflecting impaired secretory granule maturation and ER stress (7–9).

We also observed heightened autophagic flux in WFS1 SC islets, possibly induced by misfolded protein accumulation or defective insulin granule exocytosis. Secretory autophagy promotes insulin secretion in β-cells both in vivo and in vitro under high glucose conditions (30). Although autophagy is generally protective in β-cells (40,41), its overactivation may disrupt insulin availability (30,42).

GLP-1R agonists have shown promise as disease-modifying agents (17,18). Indeed, the off-label liraglutide administration to the WS1 patient under investigation improved C-peptide levels and decreased daily insulin needs (17). Consistent with the clinical data, our in vitro results show that liraglutide enhances GSIS in patient-derived SC islets by resynchronizing β-cells Ca^{2+} fluxes, regulating autophagy, and protecting against both thapsigargin- and inflammation-induced apoptosis.

Mechanistically, GLP-1R agonists are known to improve β-cell function under stress conditions. Exendin-4 reduces translational downregulation of insulin and improves cell survival in rat β-cells and in INS-1 cells upon ER stress induction (13). The GLP-1RA–mediated activation of the PI3K/Akt pathway enhances GSIS in β-cells and is critical for maintaining their survival and function (43,44).

GLP-1RAs have multiple effects on β-cells that may account for restoring the functional impairments of the endocrine compartment in WFS1 SC islets treated with

correction. *E*: Relative expression of *ATF4*, *HSPA5*, and *PDIA4* genes in WFS1 SC islets, 16 h after TG exposure ± liraglutide, and estimation plot including the mean of difference of *ATF4*, *HSPA5*, and *PDIA4* mRNAs following chronic treatment with liraglutide ($n = 3$). *$P <$ 0.05 by one-tailed *t* test. *F*: Relative expression of *ATF4, HSPA5*, and *PDIA4* genes in WFS1 SC islets, 48 h after proinflammatory cytokine exposure ± liraglutide, and estimation plot including the mean of difference of *ATF4*, *HSPA5*, and *PDIA4* mRNAs following chronic treatment with liraglutide ($n = 4$). *$P < 0.05$ by one-tailed *t* test.

liraglutide. The activation of GLP-1 signaling is known to promote *PDX1* DNA binding, driving transcription of *INS*, *MAFA*, and *PCSK1*, thus enhancing β-cell maturation that we found impaired in patient-derived SC islets (45,46). Moreover, GLP-1RAs stimulate hyperpolarization-activated cyclic nucleotide-gated channels in β- and δ-cells, thereby boosting Ca^{2+} oscillation frequency (47) and improving their regularity during the first part of the β-cell response (48). The SNARE protein complexes that mediate insulin exocytotic processes are also targets of GLP-1RAs. The phosphorylation and upregulation of SNAP25 is induced by GLP-1RA, which restores a key component of the SNARE complex (49). Indeed, we observed that liraglutide increased *CACNA1D*, *SNAP25*, and various unfolded protein response–related chaperones, probably facilitating correct protein folding and mitigating proapoptotic ER stress, thereby inducing more efficient insulin granule exocytosis. Moreover, liraglutide treatment reduces inflammatory cytokine–induced apoptosis in WFS1 SC islets, confirming the anti-inflammatory properties previously reported in other tissues (50). Exendin-4 regulates autophagic flux, lysosomal function, and cell survival in pancreatic β-cells via the RAPGEF4/EPAC2 (Rap guanine nucleotide exchange factor 4) and downstream Ca^{2+} signaling (14). Indeed, glucose-induced autophagy-mediated insulin secretion was affected by impaired Ca^{2+} flux (42).

The work described here and in the other studies mentioned above highlighted that GLP-1RAs target the cross talk between multiple cellular pathways driving GSIS and β-cell survival. This evidence supports the targeting of the GLP-1/GLP-1R axis as a therapeutic strategy for WS1. However, additional studies should dissect whether GLP-1R signaling is involved in specific *WFS1* mutation-driven defects, potentially guiding precision medicine approaches in WS1.

Acknowledgments. The authors thank the Advanced Light and Electron Microscopy BioImaging Center (ALEMBIC) at San Raffaele Scientific Institute, Milan (Italy), for assistance with confocal immunofluorescence and calcium flux recording. In particular, they acknowledge Dr. Maria Carla Panzeri and Dr. Elena Vezzoli, Alembic, Experimental Imaging Center, IRCCS San Raffaele Hospital, Milan, Italy, for their expertise in sample preparation for electron microscopy and TEM image acquisition. The authors also thank the Flow Cytometry Resource, Advanced Cytometry Technical Applications Laboratory (FRACTAL) at San Raffaele Scientific Institute, Milan (Italy), for support with FACS analysis. Furthermore, they acknowledge Dr. Francesca Giannese and Dr. Dejan Lazarevic at the Center for Omics Sciences (COSR), San Raffaele Scientific Institute, Milan (Italy), for their support in library preparation and scRNA-seq experiments, and Dr. Giulia Scotti, Centre of Omics Sciences, IRCCS San Raffaele Hospital, Milan, Italy, for scRNA-seq sample quality control and preliminary bioinformatics analysis. Finally, the authors thank Dr. Laura Monaco and Dr. Manuela Marras, Diabetes Research Institute, IRCCS San Raffaele Hospital, Milan, Italy, for their support in the latest pancreatic differentiation experiments.

Funding. This study was supported by a private family donation financing investigation on WS1 at the Diabetes Research Institute of the IRCCS San Raffaele Hospital. Part of the activities were also supported through funds from the European Union–Next Generation EU–PNRR M6C2–Investment 2.1 Enhancement and strengthening of National Health System (NHS) biomedical research (PNRR-MR1-2022-12375914).

Duality of Interest. No potential conflicts of interest relevant to this article were reported.

Author Contributions. S.T., G.S., F.C., V.Z., S.P., F.M., and R.C. performed the investigation. S.T., G.S., R.B., G.F., V.S., R.C., and L.P. contributed to reviewing the manuscript. S.T., G.S., and R.C. contributed to the methodology. S.T., G.S., and R.C. wrote the original draft. S.T., G.S., R.C., and L.P. were responsible for the formal analysis and interpretation of results. F.C., V.Z., S.P., and V.S. performed the stem cell differentiation and data analysis. R.C. conducted the bioinformatic analysis. R.C. and L.P. were responsible for conceptualization and experimental design. R.C. and L.P. supervised the study. L.P. is the guarantor of this work and, as such, had full access to all the data presented in the study and takes responsibility for the integrity of the data and the accuracy of the data analysis.

Prior Presentation. Part of this work was presented as an oral presentation at the 9th International Wolfram Syndrome Symposium, Berkshire, England, 22–24 October 2024, and the 29th Society for Investigative Dermatology National Congress, Rimini (RN), Italy, 26–29 October 2022; as a short oral presentation at the 58th European Association for the Study of Diabetes Annual Meeting, Stockholm, Sweden, 19–23 September 2022, and the 55th European Association for the Study of Diabetes Annual Meeting, Barcelona, Spain,16–20 September 2019; and as poster presentation at the PhD Symposium "INSIDE: The dark side of the cell," Wien, Austria, 11–12 February 2021, and the 28th Society for Investigative Dermatology National Congress, Rimini, Italy, 2–5 December 2020.

References

1. Rigoli L, Bramanti P, Di Bella C, De Luca F. Genetic and clinical aspects of Wolfram syndrome 1, a severe neurodegenerative disease. Pediatr Res 2018;83:921–929

2. Fonseca SG, Ishigaki S, Oslowski CM, et al. Wolfram syndrome 1 gene negatively regulates ER stress signaling in rodent and human cells. J Clin Invest 2010;120:744–755

3. Takei D, Ishihara H, Yamaguchi S, et al. WFS1 protein modulates the free Ca(2+) concentration in the endoplasmic reticulum. FEBS Lett 2006;580:5635–5640

4. Abreu D, Asada R, Revilla JMP, et al. Wolfram syndrome 1 gene regulates pathways maintaining beta-cell health and survival. Lab Invest 2020;100:849–862

5. Osman AA, Saito M, Makepeace C, Permutt MA, Schlesinger P, Mueckler M. Wolframin expression induces novel ion channel activity in endoplasmic reticulum membranes and increases intracellular calcium. J Biol Chem 2003;278:52755–52762

6. Fonseca SG, Fukuma M, Lipson KL, et al. WFS1 is a novel component of the unfolded protein response and maintains homeostasis of the endoplasmic reticulum in pancreatic beta-cells. J Biol Chem 2005;280:39609–39615

7. Shang L, Hua H, Foo K, et al. β-Cell dysfunction due to increased ER stress in a stem cell model of Wolfram syndrome. Diabetes 2014;63:923–933

8. Maxwell KG, Augsornworawat P, Velazco-Cruz L, et al. Gene-edited human stem cell-derived β cells from a patient with monogenic diabetes reverse preexisting diabetes in mice. Sci Transl Med 2020;12:eaax9106

9. Hatanaka M, Tanabe K, Yanai A, et al. Wolfram syndrome 1 gene (WFS1) product localizes to secretory granules and determines granule acidification in pancreatic beta-cells. Hum Mol Genet 2011;20:1274–1284

10. Urano F. Wolfram syndrome: diagnosis, management, and treatment. Curr Diab Rep 2016;16:6

11. Rigoli L, Caruso V, Salzano G, Lombardo F. Wolfram syndrome 1: from genetics to therapy. Int J Environ Res Public Health 2022;19:3225

12. Zheng Z, Zong Y, Ma Y, et al. Glucagon-like peptide-1 receptor: mechanisms and advances in therapy. Signal Transduct Target Ther 2024;9:234

13. Yusta B, Baggio LL, Estall JL, et al. GLP-1 receptor activation improves beta cell function and survival following induction of endoplasmic reticulum stress. Cell Metab 2006;4:391–406
14. Zummo FP, Cullen KS, Honkanen-Scott M, Shaw JAM, Lovat PE, Arden C. Glucagon-like peptide 1 protects pancreatic β-cells from death by increasing autophagic flux and restoring lysosomal function. Diabetes 2017;66:1272–1285
15. Tsuboi T, da Silva Xavier G, Holz GG, Jouaville LS, Thomas AP, Rutter GA. Glucagon-like peptide-1 mobilizes intracellular Ca2+ and stimulates mitochondrial ATP synthesis in pancreatic MIN6 beta-cells. Biochem J 2003;369:287–299
16. Panfili E, Frontino G, Pallotta MT. GLP-1 receptor agonists as promising disease-modifying agents in WFS1 spectrum disorder. Front Clin Diabetes Healthc 2023;4:1171091
17. Frontino G, Raouf T, Canarutto D, et al. Case report: off-label liraglutide use in children with Wolfram syndrome type 1: extensive characterization of four patients. Front Pediatr 2021;9:755365
18. Gorgogietas V, Rajaei B, Heeyoung C, et al. GLP-1R agonists demonstrate potential to treat Wolfram syndrome in human preclinical models. Diabetologia 2023;66:1306–1321
19. Panfili E, Mondanelli G, Orabona C, et al. Novel mutations in the WFS1 gene are associated with Wolfram syndrome and systemic inflammation. Hum Mol Genet 2021;30:265–276
20. Chimienti R, Torchio S, Siracusano G, et al. A WFS1 variant disrupting acceptor splice site uncovers the impact of alternative splicing on beta cell apoptosis in a patient with Wolfram syndrome. Diabetologia 2025;68:128–151
21. Pellegrini S, Manenti F, Chimienti R, et al. Differentiation of Sendai virus-reprogrammed iPSC into β cells, compared with human pancreatic islets and immortalized β cell line. Cell Transplant 2018;27:1548–1560
22. Muraro MJ, Dharmadhikari G, Grün D, et al. A single-cell transcriptome atlas of the human pancreas. Cell Syst 2016;3:385–394.e3
23. Baron M, Veres A, Wolock SL, et al. A single-cell transcriptomic map of the human and mouse pancreas reveals inter- and intra-cell population structure. Cell Syst 2016;3:346–360.e4
24. Daraio T, Bombek LK, Gosak M, et al. SNAP-25b-deficiency increases insulin secretion and changes spatiotemporal profile of Ca2+ oscillations in β cell networks. Sci Rep 2017;7:7744
25. Petersen MBK, Azad A, Ingvorsen C, et al. Single-cell gene expression analysis of a human ESC model of pancreatic endocrine development reveals different paths to β-cell differentiation. Stem Cell Reports 2017;9:1246–1261
26. Eliasson L, Abdulkader F, Braun M, Galvanovskis J, Hoppa MB, Rorsman P. Novel aspects of the molecular mechanisms controlling insulin secretion. J Physiol 2008;586:3313–3324
27. Rao A, McBride EL, Zhang G, et al. Determination of secretory granule maturation times in pancreatic islet β-cells by serial block-face electron microscopy. J Struct Biol 2020;212:107584
28. Ruiz de Azua I, Scarselli M, Rosemond E, et al. RGS4 is a negative regulator of insulin release from pancreatic beta-cells in vitro and in vivo. Proc Natl Acad Sci U S A 2010;107:7999–8004
29. Katsumoto K, Yennek S, Chen C, et al. Wnt4 is heterogeneously activated in maturing β-cells to control calcium signaling, metabolism and function. Nat Commun 2022;13:6255
30. Wu S-Y, Wu H-T, Wang Y-C, et al. Secretory autophagy promotes RAB37-mediated insulin secretion under glucose stimulation both in vitro and in vivo. Autophagy 2023;19:1239–1257
31. Patergnani S, Bataillard MS, Danese A, et al. The Wolfram-like variant WFS1E864K destabilizes MAM and compromises autophagy and mitophagy in human and mice. Autophagy 2024:1–12
32. Lee EM, Verma M, Palaniappan N, et al. Genotype and clinical characteristics of patients with Wolfram syndrome and WFS1-related disorders. Front Genet 2023;14:1198171
33. Huang C, Walker EM, Dadi PK, et al. Synaptotagmin 4 regulates pancreatic β cell maturation by modulating the Ca2+ sensitivity of insulin secretion vesicles. Dev Cell 2018;45:347–361.e5
34. Bader E, Migliorini A, Gegg M, et al. Identification of proliferative and mature β-cells in the islets of Langerhans. Nature 2016;535:430–434
35. Bowen A, Kos K, Whatmore J, Richardson S, Welters HJ. Wnt4 antagonises Wnt3a mediated increases in growth and glucose stimulated insulin secretion in the pancreatic beta-cell line, INS-1. Biochem Biophys Res Commun 2016;479:793–799
36. Gaisano HY. Recent new insights into the role of SNARE and associated proteins in insulin granule exocytosis. Diabetes Obes Metab 2017;19(Suppl. 1):115–123
37. Emfinger CH, Clark LE, Yandell B, et al. Novel regulators of islet function identified from genetic variation in mouse islet Ca2+ oscillations. Elife 2023;12:RP88189
38. Reinbothe TM, Alkayyali S, Ahlqvist E, et al. The human L-type calcium channel Cav1.3 regulates insulin release and polymorphisms in CACNA1D associate with type 2 diabetes. Diabetologia 2013;56:340–349
39. Gerber SH, Südhof TC. Molecular determinants of regulated exocytosis. Diabetes 2002;51(Suppl. 1):S3–S11
40. Jung HS, Chung KW, Won Kim J, et al. Loss of autophagy diminishes pancreatic beta cell mass and function with resultant hyperglycemia. Cell Metab 2008;8:318–324
41. Lee Y-H, Kim J, Park K, Lee M-S. β-cell autophagy: mechanism and role in β-cell dysfunction. Mol Metab 2019;27S(Suppl.):S92–S103
42. Jiang S, Dupont N, Castillo EF, Deretic V. Secretory versus degradative autophagy: unconventional secretion of inflammatory mediators. J Innate Immun 2013;5:471–479
43. Kaihara KA, Dickson LM, Jacobson DA, et al. β-Cell-specific protein kinase A activation enhances the efficiency of glucose control by increasing acute-phase insulin secretion. Diabetes 2013;62:1527–1536
44. Kapodistria K, Tsilibary E-P, Kotsopoulou E, Moustardas P, Kitsiou P. Liraglutide, a human glucagon-like peptide-1 analogue, stimulates AKT-dependent survival signalling and inhibits pancreatic β-cell apoptosis. J Cell Mol Med 2018;22:2970–2980
45. Abraham EJ, Leech CA, Lin JC, Zulewski H, Habener JF. Insulinotropic hormone glucagon-like peptide-1 differentiation of human pancreatic islet-derived progenitor cells into insulin-producing cells. Endocrinology 2002;143:3152–3161
46. Saikia M, Holter MM, Donahue LR, et al. GLP-1 receptor signaling increases PCSK1 and β cell features in human α cells. JCI Insight 2021;6:e141851
47. Zaborska KE, Jordan KL, Thorson AS, et al. Liraglutide increases islet Ca2+ oscillation frequency and insulin secretion by activating hyperpolarization-activated cyclic nucleotide-gated channels. Diabetes Obes Metab 2022;24:1741–1752
48. Paradiž Leitgeb E, Kerčmar J, Križančić Bombek L, et al. Exendin-4 affects calcium signalling predominantly during activation and activity of beta cell networks in acute mouse pancreas tissue slices. Front Endocrinol (Lausanne) 2023;14:1315520
49. Zhou J, Egan JM. SNAP-25 is phosphorylated by glucose and GLP-1 in RIN 1046-38 cells. Biochem Biophys Res Commun 1997;238:297–300
50. Mehdi SF, Pusapati S, Anwar MS, et al. Glucagon-like peptide-1: a multi-faceted anti-inflammatory agent. Front Immunol 2023;14:1148209

diabetes®

American Diabetes Association®

Liraglutide Treatment Reverses Unconventional Cellular Defects in Induced Pluripotent Stem Cell–Derived β-Cells Harboring a Partially Functional *WFS1* Variant

Silvia Torchio, Gabriel Siracusano, Federica Cuozzo, Valentina Zamarian, Silvia Pellegrini, Fabio Manenti, Riccardo Bonfanti, Giulio Frontino, Valeria Sordi, Raniero Chimienti, and Lorenzo Piemonti

Diabetes 2025;74(7):1273–1288 | https://doi.org/10.2337/db24-0720